XX IMEKO World Congress
Metrology for Green Growth
September 9–14, 2012, Busan, Republic of Korea

COMPARATIVE STUDY ON KINEMATIC CHARACTERISTICS OF THREE MICRO-SURGICAL MECHANISMS FOR NEUROSURGICAL OPERATIONS

S.M. Kim, J. Cheong, B.J. Yi, and W.K. Kim/Presenter

Korea University, Chochiwon, Korea, wheekuk@korea.ac.kr

Abstract: Most of commercialized micro surgical robot modules are built based on the typical 6-UPS Gough-Stewart Platform (GSP) structure. However, they may be overqualified in neurosurgical operations in aspects of workspace size, the number of motion Degree-Of-Freedoms (DOFs), and their costs. Thus, this paper suggests two different parallel mechanisms (PMs), which are a 3-UPS + PPPS type PM and a 2-UPS + PPPU type PM, as candidates for micro neurosurgical robot modules. Through a comparative study of two suggested PMs and the GSP PM in aspects of various factors such as kinematic isotropy characteristics, the workspace size required in neurosurgical operations, commercial linear actuator stroke limitations, etc., it is shown that the 2-UPS+PPPU type PMs is superior to the other two structures.

Keywords: Neurosurgical robot, parallel mechanism, stereotactic surgery, micro robot.

1. INTRODUCTION

In conventional stereotactic surgery such as Deep Brain Stimulation (DBS), the passive stereotactic surgery frame should be manually set up by the surgeon. It setup procedure could be summarized as follows. Firstly, the surgeon set up the device such that its fulcrum point coincides with the target point in the brain where electrons could be inserted [1]. This process requires adjustments of three independent 1-DOF translational motion guides. Secondly, he points the insertion needle carrying electrons to the target point on the 2-DOF rotational motion guides. Lastly, the needle can be inserted to the target point by a 1-DOF translational motion device.

In fact, most of commercialized stereotactic surgery devices have joint arrangements of either PPPRR type or PPRPR type to meet such motion requirements. Leksell stereotactic system of Elekta Medical Systems, ZD (Zamurano Duchovny) and RM stereotactic frames of Adhoc Medical, the arc-centered stereoguide of Sendstrom, CAAT Target System of Precisis AG, Aimsystem - Micromar Stereotactic System of Micromar, etc. have PPPRR type joint arrangement, while CRW Stereotactic System (Cosman-Roberts-Wells Steoreotactic Arc) of Integra LifeSciences Corporation has PPRPR type joint arrangement [2-8].

So far, various neurosurgical robot systems have been introduced which provide autonomous motion capability to reduce the setup time of the conventional stereotactic surgery frames [9-12]. In macro-micro type neurosurgical robot systems, the macro robot controls gross motions while the micro robot controls fine motions [1]. Particularly, the GSP structure is shown to be suitable for micro surgical operations [15]. In fact, most of commercialized high precision robots, which are designed suitable as micro surgical robot modules, are built with the Gough-Stewart Platform (GSP) structure such as M850 and M810 from PI Inc. [13], BORA from SYMETRIE Inc. [14], etc. However, they may be overqualified in neurosurgical operations in aspects of workspace size, the number of motion DOF, and their costs. It should be noted that conventional stereotactic surgery frames have only either PPPRR type or PPRRP type 5-DOF motion as addressed.

Thus, this paper suggests two different parallel mechanisms (PMs), which are a 3-UPS + PPPS type 6-DOF PM and a 2-UPS + PPPU type 5-DOF PM, as candidates for micro neurosurgical robot modules. Then a comparative study of these two suggested PMs and the typical GSP structure is conducted to identify the best structure as a micro surgical robot module in neurosurgical operations by considering various aspects such as kinematic isotropy characteristics, the workspace size required in neurosurgical operations, commercial linear actuator stroke limitations, etc. Note that three active prismatic joints in the PPPU type limb or in the PPPS type limb of two suggested PMs directly control 3-DOF translational motions of the PMs, and thus position analyses for those two suggested PMs could be simplified significantly, compared to the one for the typical GSP.

The paper is organized as follows. In section 2, structures of three PMs are shortly addressed and in section 3, summary on kinematic analyses of those three PMs are described. In section 4, comparative study on three PMs is conducted. Then conclusions are drawn.

2. DESCRIPTIONS OF THREE PMS

Fig. 1(a), Fig. 1(b), and Fig. 1(c), respectively, show the simplified joint arrangements for the typical GSP, a 3-UPS + PPPS type 6-DOF PM, and a 2-UPS + PPPU type 5-DOF PM. Since the GSP having identical 6 UPS type limbs as shown in Fig. 1(a) is well-known, its detailed description

and schematic are omitted here. The 3-UPS + PPPS type PM consists of a base plate, a moving plate, and three UPS type limbs and one PPPS type serial sub-chains connecting two plates. Here P, R, U, and S, respectively, represent a prismatic joint, a revolute joint, an universal joint, and a spherical joint. The 2-UPS + PPPU type PM consists of a base plate, a moving plate, and two UPS type limbs and one PPPU type serial sub-chains connecting two plates.

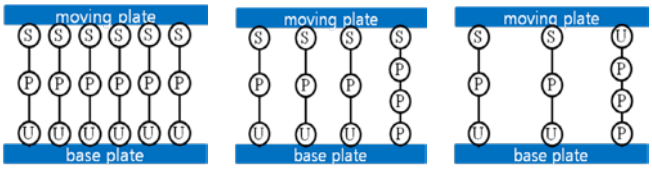

(a) (b) (c)

Fig. 1 Simplified mechanism structures: (a) typical GSP, (b) the 3-UPS + PPPS type PM, (c) the 2-UPS + PPPU type PM

Fig. 2(a) and Fig. 2(b) show schematics of the 3-UPS + PPPS type 6-DOF PM and the 2-UPS + PPPU type 5-DOF PM, respectively. As illustrated in Fig. 2(a) and Fig. 2(b), the base frames and the output frames of both the 3-UPS+PPPS type 6-DOF PM and the 2-UPS+PPPU type 5-DOF PM are defined as $(\hat{x}_b, y_b, \hat{z}_b)$ and $(\hat{x}_t, y_t, \hat{z}_t)$ at the center of the base plate and the moving plate, respectively. The PPPS type limb and the PPPU type limb of those two PMs are placed in the middle of the corresponding PM, and the last S joint and U joint of those two limbs are connected to the center of the moving plate of the corresponding PM, respectively. As shown in Fig. 2(a) all U and S joints of three UPS type limbs of the 3-UPS+PPPS type 6-DOF PM are placed symmetrically on the circles on its base plate and on its top plate, respectively. R and r, respectively, denotes the radius of the circle on the base plate and on the moving plate. All U(or S) joints of two UPS type limbs of the 2-UPS+PPPU type 5-DOF PM are placed on the circle on its base (or moving) plate with 90 degrees apart as shown in Fig. 2(b). All prismatic joints of three PMs are assumed to be actuated and l_i ($for\ i = 1,2,\cdots$) denotes the length of the i^{th} limb.

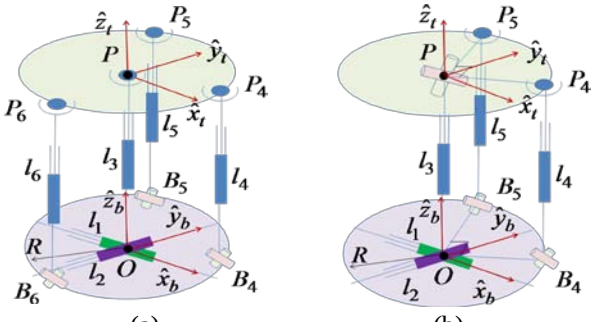

(a) (b)

Fig. 2 Schematics of two PMs : (a) the 3-UPS + PPPS type PM, (b) the 2-UPS + PPPU type PM

The global position vector from the origin of the base frame to the origin of the output frame is denoted as $\vec{R}_t = (x \quad y \quad z)^T$. The global position vector from the origin of the base frame to the U joints of the $i-th$ limb on the base plate and the global position vector from the origin of the output frame to the S joints of the $i-th$ limb on the moving plate are denoted as $\vec{R}_i = (R_{ix}, R_{iy}, R_{iz})^T$ and $\vec{r}_i = (r_{ix}, r_{iy}, r_{iz})^T$, respectively.

Now, since both PMs in Fig. 2 have either a PPPS type or a PPPU type middle chain, their input-output position equations corresponding to these middle chains can be expressed as

$$l_1 = x,\ l_2 = y,\ l_3 = z\ . \tag{1}$$

Other constraint equations related to the UPS limbs can be expressed as

$$l_i \hat{l}_i = \vec{R}_t + \vec{r}_i - \vec{R}_i\ , \tag{2}$$

where $i = 1,2,\cdots,6$ for the GSP, $i = 4,5,6$ for the 3-UPS + PPPS type PM, and $i = 4,5$ for the 2-UPS + PPPU type PM, respectively. Applying dot product of $l_i \hat{l}_i$ to both sides of (2) yields

$$\begin{aligned} l_i^2 = {} & x^2 + y^2 + z^2 + r_i^2 + R_i^2 + 2(r_{ix} - R_{ix})x + 2(r_{iy} - R_{iy})y \\ & + 2(r_{iz} - R_{iz})z + 2R_{ix}r_{ix} + 2R_{iy}r_{iy} + 2R_{iz}r_{iz}\ , \end{aligned} \tag{3}$$

Particularly, the global position vector $\vec{r}_i = (r_{ix}, r_{iy}, r_{iz})^T$ is related to the local position vector $\vec{r}_i^{(t)} = \overrightarrow{PP_i}^{(t)} = (r_{ix}^{(t)}, r_{iy}^{(t)}, r_{iz}^{(t)})^T$ as

$$\vec{r}_i = [{}_t^b R]\vec{r}_i^{(t)}. \tag{4}$$

where

$$[{}_t^b R] = [Rot(\hat{x}, \alpha)][Rot(y, \beta)][Rot(\hat{z}, \gamma)] \tag{5}$$

and

$$[{}_t^b R] = [Rot(\hat{x}, \alpha)][Rot(y, \beta)] \tag{6}$$

represent the direction cosine matrices of the output frame of the 6-DOF PMs and of the 5-DOF PM, respectively.

Thus, from (1) and (3), inverse position and angular position solutions which compute link lengths of all active prismatic joints with the given output position can be obtained. Reversely, forward position solutions which compute the output position for the given input link lengths can be found numerically from (1) and (3).

3. KINEMATICS

Direct differentiations of (1) and (2) yield

$$\dot{l}_1 = \dot{x},\ \dot{l}_2 = \dot{y},\ \dot{l}_3 = \dot{z}\ , \tag{7}$$

$$\frac{d}{dt}(l_i \hat{\hat{l}}_i) = \dot{l}_i l_i + l_i \dot{l}_i = \dot{\vec{R}}_t + \vec{\omega} \times \vec{r}_i\ , \tag{8}$$

where $\vec{\omega} = (\omega_x, \omega_y, \omega_z)^T$ denotes the global angular velocity of the output frame and is related to Euler rate vector $\dot{\vec{\mu}} = (\dot{\alpha}, \dot{\beta}, \dot{\gamma})^T$ as follows

$$\vec{\omega} = [G_\mu^\omega]\dot{\vec{\mu}}\ , \tag{9}$$

where

$$[G_\mu^\omega] = \begin{bmatrix} 1 & 0 & \sin\beta \\ 0 & \cos\alpha & -\sin\alpha\cos\beta \\ 0 & \sin\alpha & \cos\alpha\cos\beta \end{bmatrix}. \tag{10}$$

By applying a dot product of $\hat{l}_i$ to both sides of (8), the equation can be arranged with respect to the active input velocity as follows

$$\dot{l}_i = \hat{\hat{l}}_i \cdot \dot{\vec{R}}_t + (\vec{r}_i \times l_i) \cdot \vec{\omega} \,. \tag{11}$$

The inverse velocity equation of PMs can be written in a matrix form by combining (7) and (11) together as follows:

$$\dot{\vec{l}} = [G_u^l] \begin{pmatrix} \vec{v} \\ \vec{\omega} \end{pmatrix}, \quad \text{o} \quad \dot{\vec{l}}\text{r} = [G_u^l] \begin{bmatrix} I_{3\times3} & 0_{3\times3} \\ 0_{3\times3} & [G_\mu^\omega] \end{bmatrix} \begin{pmatrix} \vec{v} \\ \dot{\mu} \end{pmatrix}, \tag{12}$$

where

$$[G_u^l] = \begin{bmatrix} \vec{l}_1^T & (\vec{r}_1 \times \vec{l}_1)^T \\ \vec{l}_2^T & (\vec{r}_2 \times \vec{l}_2)^T \\ \vec{l}_3^T & (\vec{r}_3 \times \vec{l}_4)^T \\ \vec{l}_4^T & (\vec{r}_4 \times \vec{l}_4)^T \\ \vec{l}_5^T & (\vec{r}_5 \times \vec{l}_5)^T \\ \vec{l}_6^T & (\vec{r}_6 \times \vec{l}_6)^T \end{bmatrix}, \tag{13}$$

$$[G_u^l] = \begin{bmatrix} [I]_{3\times3} & [0]_{3\times3} \\ \vec{l}_4^T & (\vec{r}_4 \times \vec{l}_4)^T \\ \vec{l}_5^T & (\vec{r}_5 \times \vec{l}_5)^T \\ \vec{l}_6^T & (\vec{r}_6 \times \vec{l}_6)^T \end{bmatrix}, \tag{14}$$

and

$$[G_u^l] = \begin{bmatrix} [I]_{3\times3} & [0]_{3\times3} \\ \vec{l}_4^T & (\vec{r}_4 \times \vec{l}_4)^T \\ \vec{l}_5^T & (\vec{r}_5 \times \vec{l}_5)^T \end{bmatrix}, \tag{15}$$

are inverse Jacobian matrices for the GSP, for the 3-UPS + PPPS type PM, and for the 2-UPS+PPPU type 5-DOF PM, respectively. And $\dot{\vec{l}} = (\dot{l}_1, \dot{l}_2, \dot{l}_3, \dot{l}_4, \dot{l}_5, \dot{l}_6)^T$ and $\vec{v} = (\dot{x}, \dot{y}, \dot{z})^T$ denotes input velocity vector and output translational velocity vector, respectively.

4. COMPARATIVE STUDY ON KINEMAATIC CHARACTERISTICS

4.1 Design Parameters and Specifications

Recognizing that PMs with symmetric geometric parameters tend to show better kinematic characteristics in general, several assumptions are made for three PMs as follows. As already addressed, the GSP and the 3-UPS+PPPS type PMs are assumed to be symmetric, implying that all U joints on the base plate (or all S joints on the moving plate) are placed symmetrically on the circle of radius R (or r). But angles between two U joints on the base plate with respect to the origin of the base frame (or two S-joints on the moving plate with respect to the origin of the moving frame) for the 2-UPS+PPPU type PM are set to be 90°. Further, all design parameters of PMs are non-dimensionalized with respect to the radius of the base plate, i.e., $R = 1$. Thus design parameters of those PMs could be simplified as the radius ($r = r / R$) of the circle on the moving plate. Locations of all U joints of UPS limbs for two PMs (3-UPS +PPPS type and 2-UPS +PPPU type) are placed with appropriate fixed offsets along the z direction (z_{offset}) from the base plate.

Preliminary design specifications of PMs for the stereotactic surgery micro robot module are set as follows: total weight is less than 3Kg, translational workspace size greater than $20mm \times 20mm \times 20mm$, rotational workspace size greater than $\pm 5^\circ$ about two(or three) rotational axes, maximum linear velocity greater than $5mm/\text{sec}$, repeatability less than $0.1mm$, absolute accuracy less than $0.4mm$, compact size as possible, etc.

In fact, several commercial components are selected by taking those preliminary design criteria into account. Fig. 3 shows CAD designs of three PMs equipped with those commercially available linear actuators and linear tables. The specifications of the linear table can be summarized as follows: weight ($\le 500g$), size ($70mm \times 70mm$), stroke length ($\ge 20mm$), maximum thrust ($\ge 100N$), supporting torque about the motion axis ($\ge 500N-mm$), etc. And the specifications of the commercially available stepper-based linear actuator can be summarized as follows: weight ($\le 150g$), length ($\le 100mm$), stroke length ($\ge 25mm$), position accuracy ($\le \pm 8\mu m$), maximum thrust ($\ge 50N$), low costs, interface simplicity, etc. When both ends of the link of each UPS limb are connected to U joint and S joint as shown in Fig. 4, its length ranges from 149.5*mm* to 174.5*mm.*

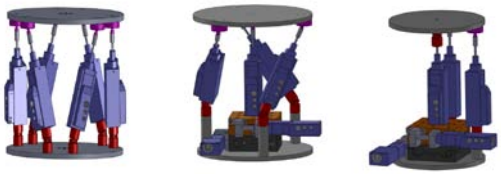

(a) (b) (c)

Fig. 3 Designs of three PMs: (a) typical GSP, (b) the 3-UPS + PPPS type PM, (c) the 2-UPS + PPPU type PM

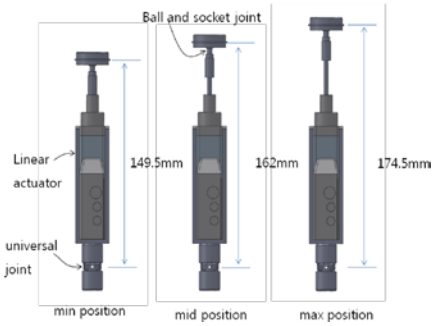

Fig. 4 Actual size and stroke lengths of the linear actuator

4.2 Kinematic Characteristics of Three PMs

Now, kinematic characteristics of three PMs are compared. As a design index, the kinematic isotropy index is used, which is defined as

$$\sigma_{KI} = \frac{\sigma_{\min}([G_l^u])}{\sigma_{\max}([G_l^u])}, \tag{16}$$

where $\sigma_{\min}([G_l^u])$ and $\sigma_{\max}([G_l^u])$ represent the minimum singular value and the maximum singular value of the

Jacobian matrix $[G_l^u]$, respectively. This index implies the directional uniformity of the output velocity to the input velocity at a configuration of the PM.

Note that it is assumed that all three PMs are designed to be symmetric as feasible, and that the desired workspace of the PMs as a stereotactic surgery micro module is very small. These conditions imply that optimal configurations lie on the vertical line passing through the origin of the base frame with the moving plate of each of three PMs parallel to its base plate. Thus, optimal design parameter for PMs could be found by searching only the translational motion space in the z direction ($x = y = 0$) and the rotational motion space about the axis of Euler angle γ ($-180^\circ \le \gamma \le 180^\circ$). Note that the rotation axis coincides with the z axis when $\alpha = \beta = 0^\circ$. Further note that it is assumed that the optimal configuration approximately represent the characteristics of the module around its vicinity which covers the whole region of the desired small workspace.

Fig. 5 shows the maximum limb length, the minimum limb length and kinematic isotropy index plot of the GSP with respect to variable z and design parameter (r/R). Each value in plots represents the optimal one found in the rotational motion space about the axis of Euler angle γ ($-180^\circ \le \gamma \le 180^\circ$). Lengths of all six limbs of the GSP for the different values of z above 0.5 turn out to be equal since the GSP is in symmetric configuration. The PM has an optimal value of kinematic isotropy index in the neighborhood of $r/R = 1$ and $z \le 0.6$ but in general its kinematic isotropy charactersitic tends to deteriorate as z increases. When the limb length is shorter such that $z \le 0.6$, the better kinematic isotropy characteristic can be secured. Note, however, that the region may not be meaningful since the configuration in the region could not be easily realized due to mechanical interferences among actual limbs.

Similarly, Fig. 6 and Fig. 7 shows the maximum limb length, the minimum limb length and kinematic isotropy index plot of the 3-UPS+PPPS type PM and the 2-UPS+PPPU type PM, respectively, with respect to variable z and design parameter (r/R). Particularly, note again that lengths of all six limbs of both PMs turn out to be equal since both PMs are in symmetric configurations.

Now, for comparison purposes, assume that actual maximum and minimum limb lengths shown in Fig. 3 are used in three PMs and that the radius of their moving plates are set as $r/R = 1$. Note that this condition makes the PMs close to symmetric as possible. In the plots, both limits of actual limb lengths are represented as bold lines in Fig. 5-Fig. 7. The unit value in plots is equivalent to 100mm in actual dimension. And for simplicity, it is assumed that the middle point between the maximum limb length and the minimum limb length is an optimal operational configuration.

As can seen in Fig. 5(c), the GSP has its optimal kinematic isotropy characteristics at $z = 1.5$ and the kinematic isotropy index value at the configuration is slightly over 0.22. Similarly, from Fig. 6(c) and Fig. 7(c), it can be observed that the optimal kinematic isotropy index values of the 3-UPS+PPPS type PM and the 2-UPS+PPPU type PM is slightly over 0.32 around $z = 1.1$ and slightly over 0.26 around $z = 1.6$, respectively. Under current assumptions and in aspects of kinematic isotropy property it can be said that the 3-UPS+PPPS type PM is the best and the GSP is the worst among three PMs. In the following, the kinematic isotropy characteristics around the optimal configurations of those three PMs as well as their workspace sizes are examined, for the cases that limits of actual limb lengths shown in Fig. 3 are used.

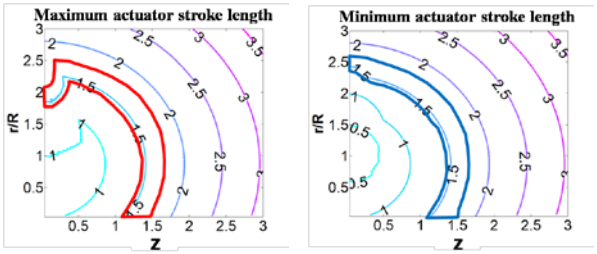

(a) (b)

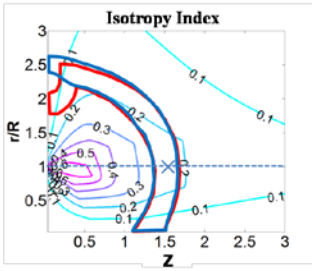

(c)

Fig. 5 a) Maximum actuator stoke length, b) minimum actuator stroke length, c) kinematic isotropy index plot of the GSP

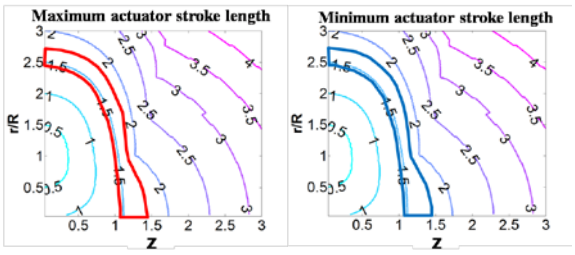

(a) (b)

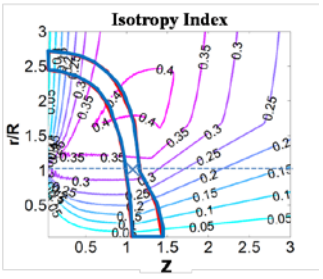

(c)

Fig. 6 a) Maximum actuator stoke length, b) minimum actuator stroke length, c) kinematic isotropy index plot of the 3-UPS+PPPS type PM

Fig. 8(a) and Fig. 8(b) show the workspace plot of the GSP type PM in the 3-DOF translational space when three rotational variables are kept fixed as $\alpha = \beta = \gamma = 0^\circ$ and the one in the 3-DOF rotational space when three translational

variables are kept as $x = y = 0$ and $z = 1.54$, respectively. Fig. 9(a) and Fig. 9(b) show the kinematic isotropy index contour plot of the GSP type PM in the $x - y$ plane for the fixed value of $z = 1.54$ with fixed rotational variables of $\alpha = \beta = \gamma = 0^\circ$ and one in the $\alpha - \beta$ plane for fixed value of $\gamma = 0^\circ$ with the fixed translational variables of $x = y = 0$ and $z = 1.54$, respectively.

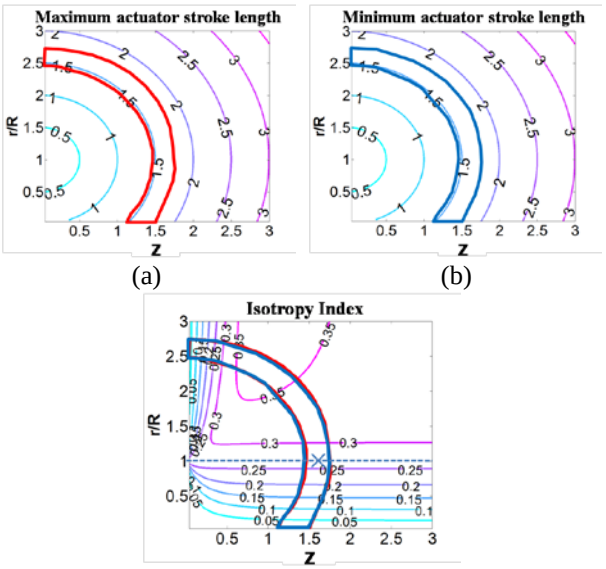

(a) (b) (c)

Fig. 7 a) Maximum actuator stoke length, b) minimum actuator stroke length, c) kinematic isotropy index plot of the 2-UPS+PPPU type PM

Fig. 10(a) and Fig. 10(b) show the workspace plot of the 3-UPS+PPPS type PM in the 3-DOF translational space when three rotational variables are kept fixed as $\alpha = \beta = 0^\circ$ and $\gamma = 72^\circ$, and the one in the 2-DOF rotational space for a fixed value of $\gamma = 72^\circ$ when three translational variables are kept as $x = y = 0$ and $z = 1.12$, respectively. Fig. 11(a) and Fig. 11(b) show the kinematic isotropy index contour plot of the 3-UPS+PPPS type PM in the $x - y$ plane for the fixed value of $z = 1.12$ with fixed rotational variables of $\alpha = \beta = 0^\circ$, and $\gamma = 72^\circ$ and the one in the $\alpha - \beta$ plane for the fixed value of $\gamma = 72^\circ$ and with fixed translational variables of $x = y = 0$, and $z = 1.12$, respectively.

Fig. 12(a) and Fig. 12(b) show the workspace plot of the 2-UPS+PPPU type PM in 3-DOF translational space when three rotational variables are kept fixed as $\alpha = \beta = \gamma = 0^\circ$ and the one in the 3-DOF rotational space when three translational variables are kept as $x = y = 0$ and $z = 1.62$, respectively. Fig. 13(a) and Fig. 13(b) kinematic isotropy index contour plot of the 2-UPS+PPPU type PM in the $x - y$ plane for the fixed value of $z = 1.62$ with the fixed rotational variables of $\alpha = \beta = \gamma = 0^\circ$ and the one in the $\alpha - \beta$ plane for the fixed value of $\gamma = 0^\circ$ with the fixed translational variables of $x = y = 0$ and $z = 1.62$, respectively.

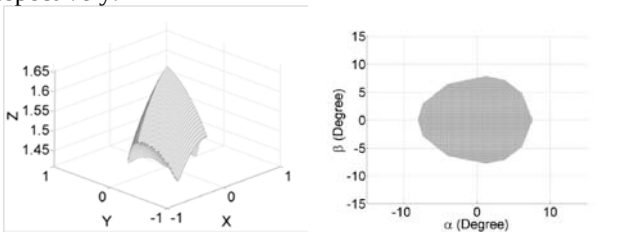

(a) (b)

Fig. 8. Workspace of the GSP type PM : (a) translational workspace when $\alpha = \beta = \gamma = 0^\circ$. (b) rotational workspace when $x = y = 0$, and $z = 1.54$.

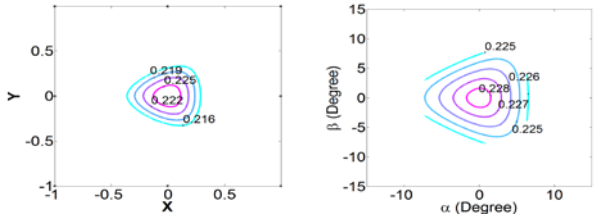

(a) (b)

Fig. 9. Kinematic isotropy index contour plots of the GSP type PM: (a) in the $x - y$ plane for fixed $z = 1.54$ and $\alpha = \beta = \gamma = 0^\circ$, and (b) in the $\alpha - \beta$ plane for fixed $\gamma = 0^\circ$, $x = y = 0$, and $z = 1.54$.

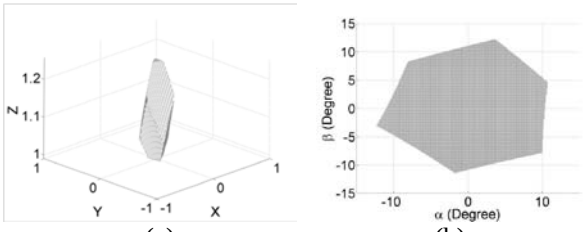

(a) (b)

Fig. 10. Workspace of the 3-UPS+PPPS type PM : (a) translational workspace when $\alpha = \beta = 0^\circ$ and $\gamma = 72^\circ$, (b) rotational workspace when $x = y = 0$, $z = 1.12$, and $\gamma = 72^\circ$.

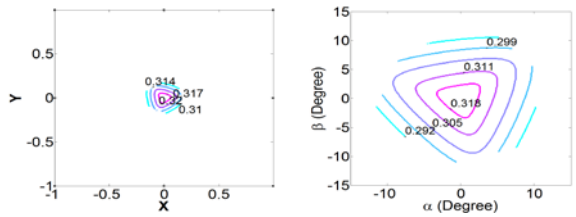

(a) (b)

Fig. 11. Kinematic isotropy index contour plots of the 3-UPS+PPPS type PM: (a) in the $x - y$ plane for fixed $z = 1.12$, $\alpha = \beta = 0^\circ$, and $\gamma = 72^\circ$, (b) in the $\alpha - \beta$ plane for fixed $\gamma = 72^\circ$, $x = y = 0$, and $z = 1.12$.

It can be seen from plots of Fig. 8 to Fig. 13 that the 2-UPS+PPPU type PM is most suitable for the stereotactic surgery micro robot module in aspects of the shape and size of workspace and kinematic isotropy characteristics. Another design aspects such as DOFs and costs need to be considered. As addressed in the introduction section, most of the conventional stereotactic surgery frames employed so

far have either the PPPRR type or PPRPR type 5-DOF joint arrangements. Thus, 5-DOF motion capability would be sufficient for the stereotactic surgery robot module. Compared with the other two designs, the 2-UPS+PPPU type PM having the PPPRR type output motion DOFs is the most compact design since it is composed of the minimum number of actuators and limbs. Thus, it can be contended that the 2-UPS+PPPU type PM be most suitable as the stereotactic surgery micro robot module among three candidate PMs.

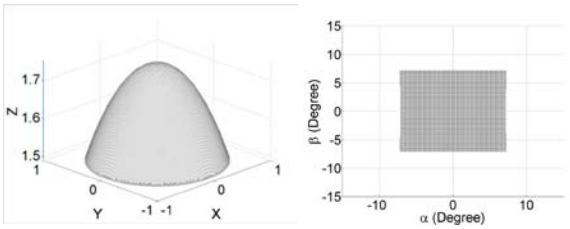

(a) (b)

Fig. 12. Workspace of the 2-UPS+PPPU type PM : (a) translational workspace when $\alpha = \beta = \gamma = 0^{\circ}$. (b) rotational workspace when $x = y = 0,\ z = 1.62,$ and $\gamma = 0^{\circ}$.

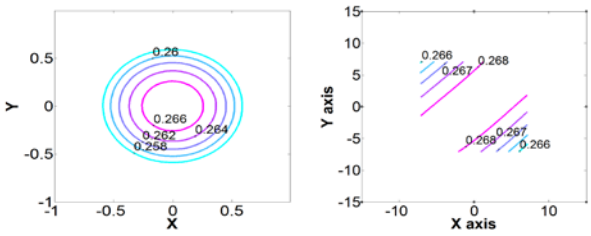

(a) (b)

Fig. 13. Kinematic isotropy index contour plots of the 2-UPS+PPPU type PM: (a) in the $x - y$ plane for fixed $z = 1.62$ and $\alpha = \beta = \gamma = 0^{\circ}$, (b) in the $\alpha - \beta$ plane for fixed $\gamma = 0^{\circ}$, $x = y = 0,$ and $z = 1.62$.

Lastly, Fig. 14 shows attachment positions of one DOF needle insertion device to the moving plate of three PMs. Note that the location of the needle insertion device on the 2-UPS+PPPU type PM needs to be arranged close to the configuration shown in Fig. 14(c) in order that the 2-DOF pitch and yaw rotational motions of the needle be secured.

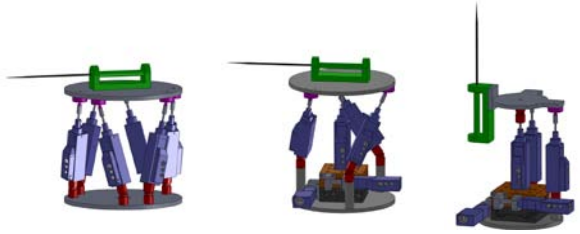

(a) GSP (b) 3-UPS+PPPS (c) 2-UPS+PPPU

Fig. 14. Locations of the needle insertion device on PMs

5. CONCLUSIONS

Two PMs (the 2-UPS+PPPU type 5-DOF PM and the 3-UPS+PPPS type 6-DOF PM), which sufficiently cover the PPPRR type output motion provided by well-recognized commercial stereotactic surgery devices, are suggested as candidates for a micro robot module in the stereotactic surgery macro-micro type robot systems. And their kinematic analyses are conducted. Noting that the motion range of the micro robot in stereotactic surgery operations is quite small, the kinematic optimizations of two suggested PMs as well as the typical GSP type PM are conducted to find their optimal operation configurations. Particularly, design specifications of the micro robot module in the stereotactic surgery macro-micro type robot systems are shortly discussed and taking the stroke length limitations of the commercial linear actuator which is selected based on desired design specifications into account, optimal operation configurations of those three PMs are selected. Then through comparative study on workspace and kinematic isotropy characteristics of those three PMs, it is shown that the 2-UPS+PPPU type PM has best characteristics than the other two PMs. Currently, constructions of the 2-UPS+PPPU type 5-DOF PM is ongoing.

ACKNOWLEDGEMENTS

This work was supported by the Technology Innovation Program (or Industrial Strategic technology development program, 10040097) funded by the Ministry of Knowledge Economy (MKE, Korea). This research was supported by the Converging Research Center Program funded by the Ministry of Education, Science and Technology (grant number, 2011K000664)

6. REFERENCES

[1] M. D. Comparetti,_ A. Vaccarella, D. Lorenzo, G. Ferrigno, and E. D. Momi, “Multi-robotic approach for keyhole neurosurgery : the ROBOCAST project,” Proceedings of the SCATH Joint Workshop on New Technologies for Computer/Robot Assisted Surgery, 2011, Graz, Austria.

[2] http://www.elektaindia.co.in

[3] http://www.adhocmedical.com/en/

[4] http://www.adhocmedical.com/en/

[5] http://www.sandstrom.on.ca

[6] http://www.precisis.de/

[7] http://www.integralife.com/

[8] www.micromar.com.br

[9] G. Cole, J. Pilitsis, and G. S. Fischer, “Design of a robotic system for MRI-guided deep brain stimulation electrode placement,” IEEE International Conference on Robotics and Automation, pp. 4450-4456, 2009.

[10] M. Heinig, M. F. Govela, F. Gasca, C. Dold, U. G. Hofmann, V. Tronnier, A. Schlaefer, and A. Schweikard, “MARS - Motor assisted robotic stereotaxy system,” IEEE EMBS Conference on Neural Engineering, pp. 334-337, 2011.

[11] A. Katashev, Y. Dekhtyar, and J. Spigulis (Eds.), “Future trends in robotic neurosurgery,” IFMBE Proceedings 20, pp. 229–233, 2008.

[12] C. S. Karas and E. A. Chiocca, “Neurosurgical robotics: a review of brain and spine applications,” J. Robotic Surg (2007) vol. pp. 39–43, 2007.

[13] http://www.physikinstrumente.com/newsletter/ausgaben_e /25/ hexapod_operation_robot.html

[14] http://www.symetrie.fr/en/positioning/

[15] M. Wapler, V. Urban, T. Weisener, J. Stallkamp, M. Dürr, and A. Hiller, “A Stewart platform for precision surgery,” Transactions of the Institute of Measurement and Control, vol. 25, no. 4, pp. 329–334, 2003.